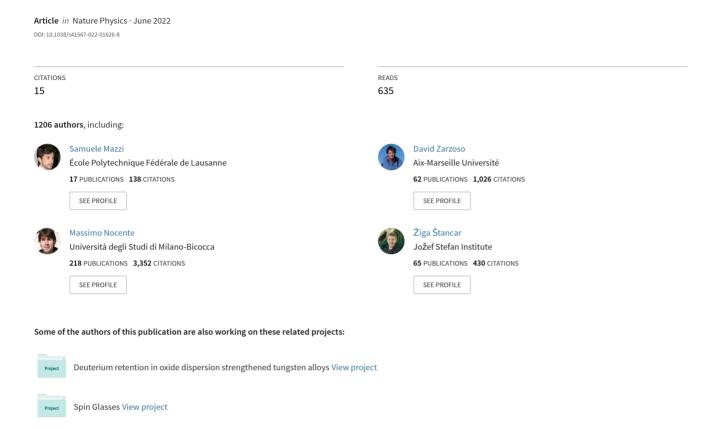
Enhanced performance in fusion plasmas through turbulence suppression by megaelectronvolt ions





Enhanced performance in fusion plasmas through turbulence suppression by megaelectronvolt ions

Samuele Mazzi, Jeronimo Garcia, David Zarzoso, Ye Kazakov, Jozef Ongena, Mykola Dreval, Massimo Nocente, Žiga Stancar, Gabor Szepesi, Jens Eriksson, et al.

▶ To cite this version:

Samuele Mazzi, Jeronimo Garcia, David Zarzoso, Ye Kazakov, Jozef Ongena, et al.. Enhanced performance in fusion plasmas through turbulence suppression by megaelectronvolt ions. Nature Physics, Nature Publishing Group, 2022, 18 (7), pp.776-782. 10.1038/s41567-022-01626-8. hal-03838301

HAL Id: hal-03838301 https://hal.archives-ouvertes.fr/hal-03838301

Submitted on 3 Nov 2022

HAL is a multi-disciplinary open access archive for the deposit and dissemination of scientific research documents, whether they are published or not. The documents may come from teaching and research institutions in France or abroad, or from public or private research centers.

L'archive ouverte pluridisciplinaire **HAL**, est destinée au dépôt et à la diffusion de documents scientifiques de niveau recherche, publiés ou non, émanant des établissements d'enseignement et de recherche français ou étrangers, des laboratoires publics ou privés.



Enhanced performance in fusion plasmas through turbulence suppression by MeV ions

S. Mazzi^{1,2,*,††}, J. Garcia^{2,**}, D. Zarzoso¹, Ye.O. Kazakov³, J. Ongena³, M. Dreval^{4,5}, M. Nocente^{6,7}, Ž. Štancar^{8,9}, G. Szepesi⁹, J. Eriksson¹⁰, A. Sahlberg¹⁰, S. Benkadda¹ and JET contributors[†]

Abstract

Alpha particles with energies of the order of MeV will be the main source of plasma heating in future magnetic confinement fusion reactors. Instead of heating fuel ions, most of the energy of alpha particles is transferred to electrons in the plasma. Furthermore, alpha particles can also excite Alfvénic instabilities, which were previously considered as detrimental for the performance of the fusion device. Here we report improved thermal ion confinement in the presence of MeV ions and strong fast ion driven Alfvénic instabilities in recent experiments on the Joint European Torus. Detailed transport analysis of these experiments reveals turbulence suppression through a complex multi-scale mechanism that generates large-scale zonal flows. This holds promise for a more economical operation of fusion reactors with dominant alpha particle heating and ultimately cheaper fusion electricity.

The urgent need for environmentally friendly energy sources becomes increasingly more important. Among several options, the fusion reaction between the hydrogen isotopes deuterium (D) and tritium (T) holds the promise for a safe clean and almost inexhaustible energy production: $D+T \to {}^{4}\text{He}$ (3.5 MeV)+n (14.1 MeV), with an alpha particle (${}^{4}\text{He}$) and a neutron (n) as fusion products. This reaction needs temperatures around 150 million K and can be realized in magnetic-confinement fusion devices [1]. The largest fusion device currently in operation is the Joint European Torus (JET) [2]. The successor device ITER aims to demonstrate the scientific and technological matureness of magnetic confinement fusion [3].

Both JET and ITER are based on the tokamak concept, a toroidal configuration schematically shown in Figure 1. Large temperature gradients (\sim 100 million K per meter) are unavoidably present in these devices because of the required high plasma temperature in the center and the necessity for a cold plasma edge. These gradients create instabilities and turbulence, often with very different spatio-temporal scale lengths [4]. One of the most important is the ion temperature gradient (ITG) instability with a characteristic scale length on the order of the ion gyroradius, usually much smaller than the plasma size (e.g., \sim 10⁻³ m vs. \sim 1 m in JET). The microscopic ITG instability largely limits plasma temperatures that can be achieved in a fusion device [5].

The success of magnetic confinement fusion as an energy source relies crucially on reaching high temperatures for the D and T ions. Fusion-born MeV-range alpha particles are the main source of central plasma heating in ITER and future fusion power plants. Yet, these highly energetic ions heat primarily electrons rather than thermal ions through Coulomb collisions. The extrapolation of plasma heating by alpha particles in future devices is not

¹ Aix-Marseille Université, CNRS PIIM, UMR 7345 Marseille, France

² CEA, IRFM, F-13108 Saint-Paul-lez-Durance, France

³ Laboratory for Plasma Physics, LPP-ERM/KMS, TEC Partner, BE-1000 Brussels, Belgium

⁴Institute of Plasma Physics, National Science Center, Kharkiv Institute of Physics and Technology, Kharkiv, Ukraine

⁵ V.N. Karazin Kharkiv National University, Kharkiv, Ukraine

 $^{^6}$ Dipartimento di Fisica "G. Occhialini", Università di Milano-Bicocca, Milan, Italy

⁷ Institute for Plasma Science and Technology, National Research Council, Milan, Italy

 $^{^8\,}Jožef\,\,Stefan\,\,Institute,\,\,Jamova\,\,cesta\,\,39,\,\,SI\text{-}1000\,\,Ljubljana,\,\,Slovenia$

⁹ CCFE, Culham Science Centre, Abingdon, Oxon, OX14 3DB, United Kingdom

¹⁰Department of Physics and Astronomy, Uppsala University, Uppsala, Sweden

[†] See the author list of "Overview of JET results for optimising ITER operation" by J. Mailloux et al., (2022) Nucl. Fusion in press

^{*} \pmb{Email} : samuele.mazzi@univ-amu.fr

^{††}now at: Ecole Polytechnique Fédérale de Lausanne (EPFL), Swiss Plasma Center, CH-1015 Lausanne, Switzerland

^{**} Email: jeronimo.garcia@cea.fr

straightforward partly because of the impact of fast ions on plasma turbulence. Recent progress in this developing field of research showed that ion scale turbulence can be partly reduced in the presence of fast ions with energies of ~ 100 keV [6–9]. However, at these energies fast ions provide dominant bulk ion heating in strong contrast to electron heating from alphas in a fusion reactor.

Alpha particles can also excite a range of instabilities, which are often considered detrimental for plasma confinement. Modes driven by fast ions can cause increased radial transport of energetic ions [10–13] and enhance plasma turbulence [14]. Among possible instabilities driven by alpha particles in ITER, toroidicity-induced Alfvén eigenmodes (TAEs) [15, 16] are of particular concern [17]. Yet numerical analysis in [9] showed that in plasmas with ion heating from \sim 100 keV ions, i.e. under conditions far from those in a fusion reactor, reduced turbulence can be obtained when TAEs are marginally stable, leaving the question open on whether improved thermal ion confinement can be reached experimentally in plasmas with MeV-range fast ions and fully destabilized TAEs.

Thermal ion energy fluxes perpendicular to the magnetic surfaces can be reduced because of the appearance of intense poloidally directed shear flows, known as zonal flows [18]. In fact, zonal flows, which are solely generated by nonlinear interactions, are a common phenomenon in nature and can be remarkably stable as, e.g., the famous belts of Jupiter [19]. The generation of zonal flows by energetic ions and fast ion driven modes, in particular TAEs, was put forward in simplified contexts in several theoretical studies recently [20, 21]. As the dynamics of ITER plasmas will be determined in part by the nonlinear interaction between MeV-range alphas, Alfvén eigenmodes destabilized by these alphas, and microturbulence, studying this complex interplay at ITER-relevant conditions becomes an urgent necessity for future progress in fusion science.

In this paper, we identify reproducible conditions and provide experimental evidence for the suppression of ion-scale turbulence in fusion-reactor-grade plasmas with strong electron heating from MeV-range fast ions and simultaneously destabilized Alfvén eigenmodes. Corroborated by detailed turbulence analysis, our results pave the way towards enhanced performance of future fusion reactors with strong alpha particle heating.

Improved thermal ion confinement in plasmas with MeV ions

The impact of fast ions on plasma dynamics was studied in JET D-³He plasmas $(n(^3\text{He})/n_e \approx 20\text{-}30\%)$. While the presence of TAEs is usually accompanied by a loss of energy and particle confinement [10,11,22–24], here we show that reduced ion heat losses and high ion temperatures can be reached in plasmas with MeV-range fast ions and TAEs driven by fast ions. Figure 2 compares JET pulses #94704 (~100 keV ions; blue lines) and #94701 (MeV-range ions; red lines) that were performed at the same operational parameters (L-mode, $B_0 = 3.7 \text{ T}$, $I_p = 2.5 \text{ MA}$, $n_{e0} \approx 6 \times 10^{19} \text{ m}^{-3}$) and total auxiliary heating power $P_{\text{aux}} = 14 \text{ MW}$, but differing in the characteristics of the fast ion population.

In pulse #94704 (blue lines in Fig. 2), Neutral Beam Injection (NBI) was the only heating system, providing fast D ions with energies up to 100 keV. These moderately energetic ions deposit most of their energy to bulk ions, resulting in plasmas with $T_i/T_e > 1$ (e.g., $T_i/T_e \approx 1.4$ measured at $\rho_{\rm tor} = 0.2$). The corresponding electron and ion temperature profiles at $P_{\rm aux} = 14$ MW (t = 9.0 s) are shown in Figs. 2(f) and (g). The injected fast NBI ions are sub-Alfvénic ($v_{\rm NBI}/v_{\rm A} \approx 0.4$) and no Alfvén eigenmodes were observed in this plasma.

In the comparison pulse #94701 (red lines in Fig. 2), fast D ions from NBI were accelerated to much higher energies (up to ~2-3 MeV; see Fig. S1 in the Supplementary Information) with waves in the ion cyclotron range of frequencies (ICRF) using the three-ion D-(D_{NBI})- 3 He scheme ($P_{\rm NBI}=8$ MW, $P_{\rm ICRF}=6$ MW) [25–28]. The presence of MeV-range ions resulted simultaneously in long-period sawteeth, destabilization of various Alfvén eigenmodes, as well as in the increased plasma stored energy and D-D neutron rate. As a result of the collisional slowing-down, these highly energetic deuterons heat predominantly electrons (similar to alpha particle heating in future fusion reactors), giving rise to a strongly peaked electron temperature profile with much larger T_{e0} , see Fig. 2(f). Interestingly, the ion temperature in this core-electron-heated plasma was at least as high as in the NBI-only pulse #94704 with more ion heating and $T_i/T_e \approx 1$ was reached.

We focus on the transport characteristics in the central region of these plasmas ($\rho_{tor} \lesssim 0.4$), where most of the alpha particles will be generated in a future fusion reactor. The electron and thermal ion heat diffusivities computed with TRANSP [29,30], see Figures 2(h) and (i), show that ions are the primary heat loss channel in the NBI-only pulse #94704 ($\chi_i > \chi_e$): e.g., at $\rho_{tor} = 0.23$, $\chi_i \approx 1.9$ m² s⁻¹ and $\chi_e \approx 0.6$ m² s⁻¹. In contrast, in pulse #94701 with highly energetic ions, $\chi_i \approx 0.8$ m² s⁻¹ is much reduced at this radial location, while χ_e remains almost unchanged. The comparison of two χ_i -profiles shown in Fig. 2(i) clearly indicates a significant improvement of thermal ion confinement in the plasma core of the pulse with electron heating by fast ions. Note that in the absence of ion temperature measurements at $\rho_{tor} < 0.2$, the near-axis χ_i were computed using a global third-order polynomial fit for T_i (routinely employed in TRANSP modelling of JET experiments), or assuming $T_i = T_e$; see the Methods section.

As a next step, predictive modeling of T_i in pulse #94701 was undertaken with the CRONOS code [31], using all relevant parameters, including measured T_e and n_e , and heat source profiles calculated by TRANSP as input. Two different χ_i -profiles were assumed in this analysis, see Fig. 2(i). The impact of the reduced ion heat losses on the achieved T_i in #94701 is clearly illustrated by comparing the two predicted T_i -profiles shown in Fig. 2(g). The red dotted line illustrates the predicted ion temperature in #94701 using the TRANSP-computed χ_i for this pulse. The good agreement of the predicted and measured T_i profiles verifies the consistency of CRONOS and this synthetic modelling approach. This analysis also shows that a much lower T_i would have been reached in #94701 (red dashed line), if the thermal ion heat diffusivity were the same as in the NBI-only pulse #94704. However, the experimentally observed T_i in #94701 is significantly larger than the latter T_i prediction, another confirmation for reduced ion heat losses in the presence of MeV ions.

The well-known mechanisms stabilizing ITG turbulence such as the ratio T_i/T_e and the $E \times B$ shearing rate $(\gamma_{E \times B})$ cannot explain the lower χ_i in the core region $\rho_{\rm tor} < 0.4$ for pulse #94701. Indeed, both parameters are lower in this pulse as compared to those in the NBI-only pulse #94704: e.g., at $\rho_{\rm tor} = 0.23$, $T_i/T_e \approx 1$ vs. 1.4 and $\gamma_{E \times B} \approx 1.4$ ms⁻¹ vs. 2.2 ms⁻¹.

The two comparison pulses are not only inherently different in the heating channel for fast ions (dominant ion vs. electron heating), but also feature an essential difference in the MHD behavior. The sub-Alfvénic NBI ions in #94704 did not destabilize any Alfvén eigenmodes. In contrast, a variety of TAE modes in the frequency range ~200 kHz with toroidal mode numbers n=2-6 were driven by high-energy ions in pulse #94701, see Fig. 2(e). The observed mode frequencies are in good agreement with the theoretically predicted frequencies of TAEs, $f_{\rm TAE}^{\rm (lab)} = f_{\rm TAE}^{\rm (plasma)} + nf_{\rm rot}$. In this formula, $f_{\rm TAE}^{\rm (plasma)} = v_{\rm A0}/(4\pi q_{\rm TAE}R_0) \approx 166-191$ kHz, $q_{\rm TAE} \simeq 1+1/(2n) \approx 1.1-1.3$ [24], $v_{\rm A0}$ is the Alfvén velocity in the plasma center, and $f_{\rm rot} \approx 7-8$ kHz is the local plasma rotation frequency, as measured by the CXRS system. The localization of TAEs outside the q=1 surface in this ICRF+NBI plasmas has been independently confirmed by correlation reflectometer measurements, indicating that $R_{\rm TAE} \approx 3.22-3.36$ m (see Fig. S3(a) in the Supplementary Information).

The correlation reflectometer also provides local density fluctuation spectra, used to characterize the turbulence characteristics in the plasma. The performed analysis at R=3.25 m and R=3.3 m (see Figs. S3(b) and (c) in the Supplementary Information) highlights that the lowest fluctuation amplitudes were reached in plasmas with MeV-range fast ions and destabilized TAEs. Furthermore, a clear reduction of the thermal ion heat diffusivity was observed at these radial locations, see Fig. 2(i). As the characteristics of the fast ions in pulse #94701 ($T_{\rm fast}/T_e \approx 34$ and $n_{\rm fast}/n_e \approx 3\%$) are close to the predicted conditions for alpha particles in ITER [32], the identified mechanism holds promise for optimizing the performance of future fusion reactors with strong alpha-particle heating.

Note that the observed sawtooth dynamics in pulse #94701 is similar to earlier JET experiments with ICRF and monster sawteeth reported in [33,34]. However, in strong contrast to [33], a much smaller plasma volume was enclosed within the sawtooth inversion radius in the JET experiments reported here, thereby limiting the impact of the sawtooth stabilization itself on the improved plasma confinement. We also note that the power balance analysis used in this paper to infer the thermal conductivities ignores any possible anomalous ion heating effects such as, e.g., reported in [35]. In the absence of reliable measurements of high-frequency Alfvén eigenmodes (> 1 MHz), their potential impact in the reported plasmas is difficult to assess.

Numerical modeling of turbulence suppression

These JET experimental observations are corroborated by modelling with the local (or 'flux-tube') version of the state-of-the-art gyrokinetic code GENE [36] that successfully reproduced turbulence properties for various tokamak experiments (see e.g. Refs. [6,7,37–39]). For analysis of JET pulse #94701, we choose a flux-tube around $\rho_{\text{tor}} = 0.23$ (R = 3.25 m) as this region is characterized by large temperature gradients and a significant population of fast ions and TAEs. Table 1 summarizes the modelling input data. An equivalent Maxwellian distribution was used to represent the population of fast deuterons. Linear stability analysis shows that, as expected, ITG modes dominate the spectrum, peaking at $k_y \rho_s \approx 0.45$. Here, k_y is the binormal ('poloidal') wavenumber and ρ_s is the characteristic Larmor radius of thermal ions at the reference sound speed defined in this paper as $c_s = (T_e/m_p)^{1/2}$ with m_p the proton mass.

Because of the uncertainties in the fast ion profiles calculated by TRANSP in the presence of destabilized Alfvén eigenmodes and limitations of the Maxwellian approximation to represent fully the detailed fast ion distribution, a scan over the normalized fast ion logarithmic pressure gradient, $R/L_{p_{\rm FD}}$ was performed. This allows to compensate the discrepancy induced by the derivative in velocity space by fine-tuning the radial gradient of the fast ion temperature and density profiles. Furthermore, as a part of this assessment, we find that for $R/L_{p_{\rm FD}} > 10.7$ fast D ions destabilize ballooned modes with frequencies $f \approx 200$ kHz and $k_u \rho_s$ between 0.025 and 0.05, corresponding

to n=4-7. As all these mode characteristics match well with those of the experimentally measured TAEs (Figure 2(e)), these high-frequency modes appearing in the GENE simulations are identified as fast-ion-driven TAEs.

This analysis was followed by nonlinear GENE simulations. Figure 3(a) shows the heat diffusivity attributed to electrostatic fluctuations for both thermal ion species, $\chi_{\rm ES}({\rm D})$ and $\chi_{\rm ES}(^3{\rm He})$. Figures 3(b)-(d) illustrate the amplitudes of the Fourier components normalized to their maximum, $\hat{\phi}_n$ of the perturbed electrostatic potential ϕ (averaged over the radial and parallel directions) as a function of frequency and $k_y \rho_s$. The frequency dependence of $\hat{\phi}_n$, additionally averaged over $k_y \rho_s$, is illustrated in Figures 3(e)-(g). The turbulence spectra reveal that for $R/L_{p_{FD}} \approx 6$, the dominant modes are characterized by low frequencies and peak around $k_y \rho_s \approx 0.2$. These k_y values are somewhat lower than in linear simulations. This is typical for a local gyrokinetic modelling and linked to the inverse cascade of energy, in which modes with larger k_y transfer energy to modes with lower k_y . At larger fast ion gradients, e.g. at $R/L_{p_{FD}} \approx 16$, the turbulence structure is substantially modified. The dominant modes are shifted towards higher frequencies $f \approx 200$ kHz and lower $k_y \rho_s \approx 0.025 - 0.05$, matching closely the characteristics of the observed TAEs.

Figure 3(a) clearly shows a strong stabilizing effect of fast ions on ion-scale turbulence when fast ion driven TAEs appear in nonlinear GENE simulations; see, e.g., Figure 3(g) computed for $R/L_{pFD} \approx 16$. Under these conditions, the computed diffusivities of both thermal ion species are reduced by more than 95% compared to the values obtained without fast ions, and agree well with χ_i computed by TRANSP (the black dashed line in Figure 3(a)). However, the predicted GENE value $\chi_e \approx 3.5 \text{ m}^2 \text{ s}^{-1}$ is significantly larger than the electron heat diffusivity from TRANSP ($\chi_e \approx 0.5 \text{ m}^2 \text{ s}^{-1}$). To obtain better agreement between GENE and power balance results, an additional set of non-linear simulations was performed, by varying the input parameters within experimental uncertainties. The consistency in both χ_i and χ_e was simultaneously achieved at $R/L_{pFD} \approx 14$ with temperature gradients reduced by 15%, see Figure 3(c) and (f), yielding $\chi_e \approx 0.7 \text{ m}^2 \text{ s}^{-1}$. This result supports the observation of high T_{e0} in JET pulse #94701, in contrast to earlier NSTX results where the electron confinement was strongly degraded in the presence of Alfvén eigenmodes [40].

We note that modes at $f \approx 20-30$ kHz were observed in #94701. Modes at similar frequencies also appeared in Gene simulations at $R/L_{p_{FD}} \approx 14$ and 16. The bispectral analysis of the electrostatic potential indicates a nonlinear coupling between these modes and TAEs, similar to results reported in [41]. However, since turbulence suppression is reached in Gene simulations already at $R/L_{p_{FD}} \approx 11$, when such a mode coupling is not observed, we exclude these low-frequency-modes as a main cause for the observed confinement improvement.

Figures 4(a)-(c) illustrate the dependence of the perturbed electrostatic potential ϕ on the radial (x/ρ_s) and binormal (y/ρ_s) coordinates. In the absence of fast ions (Fig. 4(a)), small-scale turbulent eddies predominately elongated along the radial direction, typical for ITG-induced transport, are seen. In contrast, Figs. 4(b) and (c) show the sudden appearance of intense poloidally-oriented and radially-sheared zonal flows in GENE simulations at $R/L_{p_{FD}} \approx 14$ and $R/L_{p_{FD}} \approx 16$, corresponding to plasmas with MeV ions and destabilized TAEs. In these cases, the zonal flow shearing rate respectively reaches $\gamma_{E\times B,\, zonal} \approx 0.84 \, c_s/a$ and $0.86 \, c_s/a$, almost twice the value without fast ions $(0.48 \, c_s/a)$. These zonal flows strongly affect the ITG nonlinear saturation [18] and produce a radial de-correlation of the turbulent eddies [42], thereby leading to a reduction in the turbulent transport. Furthermore, Figs. 4 (e)-(f) illustrate the appearance of zonal structures also in the perturbed magnetic potential with unstable TAEs, consistent with earlier analytical studies [21]. The strong coupling between fast ion driven modes and zonal components, previously shown in simplified contexts [20,21], is further highlighted by the bispectral analysis. This analysis suggests a net energy transfer from TAEs to the zonal modes, see Supplementary Figure S6.

The robustness of GENE results was further checked against the uncertainty in the input R/L_{T_i} , arising from a lack of T_i data at $\rho_{\text{tor}} < 0.2$ (see also Methods). The mechanism is reproducible and robust against unavoidable assumptions and simplifications of the local approach.

Experimental evidence for minimized density fluctuations

Modeling predictions of the turbulence suppression are supported by the observation of reduced amplitude of the density fluctuations in these JET plasmas, in particular, in pulse #95669 performed at very similar plasma conditions as #94701. Figures S3(b) and (c) in the Supplementary Information show that much smaller density fluctuation amplitudes were observed in the plasma phase with MeV-range fast ions and fast ion driven TAEs, as compared to the NBI-only phase. As outlined earlier, partial turbulence reduction in the presence of moderately energetic ions (of a few hundred keV) does not necessarily require TAEs and has been extensively reported [6–9]. This has also been observed in this series of JET experiments, e.g. in pulse #95672 (see Supplementary Fig. S3), where the application of the three-ion scheme with $P_{\rm ICRF} = 2.1$ MW resulted in monster sawteeth, while TAEs

were not destabilized. However, a much stronger reduction was measured in the same JET pulse when ICRF power was increased to 6 MW such that MeV-range ions and fast ion driven TAEs were present in the plasma. Supplementary Figure S4(c) clearly illustrates the efficacy of the turbulence suppression mechanism discovered in these JET experiments.

A promising result for ITER and future fusion devices

These promising JET results indicate that unexpected favourable conditions might be realized in ITER and future fusion power plants, where alpha particles provide a strong source of core electron heating [43]. As fast alphas can simultaneously destabilize TAEs at large plasma volumes in ITER [17], this complex mechanism – if present – would provide a significant increase in plasma confinement. However, TAEs can also enhance the fast particle transport, and thus the final result would depend on a delicate balance between different competing effects. Predicting the actual TAE mode stability and the efficiency of turbulence suppression in ITER plasmas is challenging because of the sensitivity to radial profiles of background quantities or the energetic particle distributions. Therefore, whether this favorable mechanism of turbulence stabilization will actually materialize in ITER plasmas is an open question. However, the results shown in this paper pave the way to an enhanced realization of fusion as an energy source, which is worth exploring further both experimentally and theoretically in the future.

Acknowledgements

We thank Matteo Baruzzo and Filomena Nave for the preparation and execution of JET experiments discussed in this paper; Elena de la Luna for her support in detailing the experimental diagnostics of JET; Aaron Ho for his assistance in processing the experimental data; Tobias Görler for providing an essential advice to ensure the correct numerical setup for the GENE modeling reported in this paper; Yann Camenen, Xavier Garbet and Andreas Bierwage for fruitful discussions about the gyrokinetic analyses; Gerardo Giruzzi for valuable suggestions on the article strategy. The simulations were performed on IRENE Joliot-Curie HPC system, in the framework of the PRACE projects IONFAST and AFIETC, and on CINECA Marconi HPC within the project GENE4EP.

This work has been carried out within the framework of the EUROfusion Consortium and has received funding from the Euratom research and training programme 2014–2018 and 2019–2020 under Grant agreement No 633053. The views and opinions express herein do not necessarily reflect those of the European Commission. Part of the work by Ye.O.K. and J.O. was also carried out in the framework of projects done for the ITER Scientist Fellow Network (ISFN).

Author Contributions

The reported JET experiments were designed and coordinated by Ye.O.K., M.N., J.G. and J.O.; S.M. performed gyrokinetic simulations and subsequent analysis, with support of J.G., D.Z. and S.B.; input data for gyrokinetic modeling were provided by Ž.Š., G.S., Ye.O.K. and M.D.; Ž.Š. performed TRANSP modeling; J.G. performed power balance analysis and CRONOS simulations; M.D. provided analysis of the TAE radial location and the correlation reflectometer data; J.E. and A.S. provided neutron measurements data from TOFOR. The original manuscript was written by S.M., J.G., Ye.O.K., J.O. and D.Z. with feedback by all the authors. Major revisions of this manuscript were written by Ye.O.K., J.O., J.G. and S.M.

Competing Interests

The authors declare no competing interests.

Tables

Table 1: Plasma parameters used in the GENE modelling of JET pulse #94701 at $\rho_{tor} = 0.23$ and $t \approx 9.6$ s.

Here, R_0 is the major radius, B_0 the on-axis magnetic field, ϵ the inverse aspect ratio, q and \hat{s} the local safety factor and magnetic shear, n_j and T_j the local density and temperature of various plasma species (electrons, thermal D and ³He ions, fast D ions), $R/L_{n,T}$ the normalized logarithmic density and temperature gradient, β_e the electron-beta, ν^* the normalized collision frequency. The reported input parameters are common to all the numerical GENE simulation cases. The various cases, however, differ essentially in the fast ion pressure gradient $R/L_{p_{\rm FD}}$, whose values are displayed e.g. in Figure 3.

Figure Legends/Captions

Figure 1: Schematic view of the tokamak geometry. In tokamaks, charged particles are confined by a combination of toroidal and poloidal magnetic fields that generate nested surfaces of constant magnetic flux. Passing particles (blue trajectory) circulate along magnetic field lines in the toroidal direction φ , while trapped particles (red trajectory) periodically reverse their parallel velocity with respect to the confining magnetic field \vec{B} . For simplicity, the rapid gyromotion of charged particles is not shown and only the guiding center motion is displayed. In this paper, the local transport analysis focuses on the magnetic flux surface corresponding to $\rho_{\text{tor}} = 0.23$ (in green), where ρ_{tor} is the square root of the toroidal magnetic flux normalized to its value at the plasma boundary. The top left inset illustrates the field-aligned set of coordinates used in the flux-tube version of the GENE code, with (x, y, z) the radial, binormal and parallel coordinate, respectively. The top right inset shows a poloidal cross-section of the plasma in the (R, \mathbb{Z}) plane for the reported JET experiments, together with the studied flux surface $\rho_{\text{tor}} = 0.23$ (green) and the plasma boundary $\rho_{\text{tor}} = 1$ (grey). Here, R is the radial distance from the torus centre and \mathbb{Z} is the vertical coordinate. Note that $\rho_{\text{tor}} = 0.23$ corresponds to R = 3.25 m at the outboard side.

Figure 2: Improved thermal ion confinement in fusion plasmas with MeV ions and unstable TAEs. This is illustrated by comparing two JET pulses #94704 (~100 keV ions; blue lines) and #94701 (MeV-range ions; red lines) performed at the same operational conditions and the same total auxiliary heating power $P_{\text{aux}} = 14$ MW, but differing in the characteristics of the fast ion population. (a) NBI and ICRF power. (b) Core electron temperature T_{e0} . (c) Plasma stored energy W_p . (d) Neutron rate from D-D fusion reactions. (e) The magnetic coil spectrogram showing destabilized TAEs with different toroidal mode numbers, n in pulse #94701. Panels (f) and (g) show the measured radial profiles of the electron, T_e and ion temperatures, T_i at $P_{\text{aux}} = 14$ MW. The error bands in both panels represent a combination of the systematic diagnostic uncertainties and time-averaged (± 0.1 s) statistical variations of the measurements. Panels (h) and (i) display the computed electron, χ_e and thermal ion, χ_i heat diffusivities. The error bands in these panels take into account uncertainties in the temperature profile data, different fittings to T_i and its extrapolation to the magnetic axis, including uncertainties in the power balance. The red dotted and dashed lines in (g) show the predicted T_i profiles for pulse #94701, using the two χ_i profiles from panel (i) as input.

Figure 3: Thermal ion transport suppression in plasmas with MeV ions and fast ion driven modes. (a) The electrostatic thermal diffusivities of D and 3 He ions against the fast ion pressure gradient $R/L_{p_{\rm FD}}$ as predicted by Gene. (b-d) Contour plots of the Fourier components normalized to their maximum, $\hat{\phi}_n$ of the perturbed electrostatic potential ϕ (averaged over the radial and parallel directions) as a function of frequency and $k_y \rho_s$. (e-g) The frequency dependence of $\hat{\phi}_n$, additionally averaged over $k_y \rho_s$ (indicated by the symbol $\langle ... \rangle$). In (f) and (g), the grey shaded areas indicate the experimentally measured TAE frequency range. In panel (a), the error bars of Gene time-dependent simulations represent the standard deviation obtained from the code calculation. The large error bars for the rightmost points can be attributed to the high-frequency and large-amplitude modulations of the energy fluxes due to strong fast ion driven fluctuations of the electrostatic potential. The horizontal dotted lines and the associated shaded areas in panel (a), represent thermal ion diffusivities and their standard deviations for the Gene modelling case without fast ions. The dashed line at the bottom of panel (a) shows the computed thermal ion heat diffusivity for JET pulse #94701, $\chi_i = 0.8 \text{ m}^2 \text{ s}^{-1}$, as given by TRANSP, with the grey shaded area corresponding to the error band in Fig. 2(i).

Figure 4: Evidence for the nonlinear generation of zonal structures. Contour plots of the gyroaveraged perturbed electrostatic potential, ϕ , and the component of the vector potential parallel to the magnetic field, $A_{||}$, for different fast ion pressure gradients $R/L_{p_{FD}}$ along the radial x and binormal y components. Panels (a) and (d) correspond to the modeling case without fast ions; panels (b) and (e) for the fast ion case with $R/L_{p_{FD}} \approx 14$; panels (c) and (f) for the fast ion case with $R/L_{p_{FD}} \approx 16$. All contour plots are normalized to the corresponding maximum value. This figure clearly shows the appearance of zonal structures leading to turbulence suppression in plasmas with MeV-range ions and fast ion driven TAEs.

References

- [1] Ongena, J., Koch, R., Wolf, R. & Zohm, H. Magnetic-confinement fusion. *Nat. Phys.* **12**, 398–410 (2016). URL https://doi.org/10.1038/nphys3745
- [2] Litaudon, X. et al. Overview of the JET results in support to ITER. Nucl. Fusion 57, 102001 (2017). URL https://doi.org/10.1088/1741-4326/aa5e28
- [3] Shimada, M. et al. Chapter 1: Overview and summary. Nucl. Fusion 47, S1–S17 (2007). URL https://doi.org/10.1088/0029-5515/47/6/S01
- [4] Doyle, E. J. et al. Chapter 2: Plasma confinement and transport. Nucl. Fusion 47, S18 (2007). URL https://doi.org/10.1088/0029-5515/47/6/S02
- [5] Romanelli, F. Ion temperature-gradient-driven modes and anomalous ion transport in tokamaks. *Phys. Fluids B: Plasma Physics* 1, 1018–1025 (1989). URL https://doi.org/10.1063/1.859023
- [6] Citrin, J. et al. Nonlinear stabilization of tokamak microturbulence by fast ions. Phys. Rev. Lett. 111, 155001 (2013). URL https://doi.org/10.1103/PhysRevLett.111.155001
- [7] Garcia, J. et al. Key impact of finite-beta and fast ions in core and edge tokamak regions for the transition to advanced scenarios. Nucl. Fusion 55, 053007 (2015). URL https://doi.org/10.1088/0029-5515/55/5/ 053007
- [8] Di Siena, A., Görler, T., Doerk, H., Poli, E. & Bilato, R. Fast-ion stabilization of tokamak plasma turbulence. Nucl. Fusion 58, 054002 (2018). URL https://doi.org/10.1088/1741-4326/aaaf26
- [9] Di Siena, A. et al. Electromagnetic turbulence suppression by energetic particle driven modes. Nucl. Fusion 59, 124001 (2019). URL https://doi.org/10.1088/1741-4326/ab4088
- [10] Fasoli, A. et al. Chapter 5: Physics of energetic ions. Nucl. Fusion 47, S264 (2007). URL https://doi.org/ 10.1088/0029-5515/47/6/S05
- [11] Gorelenkov, N., Pinches, S. D. & Toi, K. Energetic particle physics in fusion research in preparation for burning plasma experiments. Nucl. Fusion 54, 125001 (2014). URL https://doi.org/10.1088/0029-5515/ 54/12/125001
- [12] Todo, Y. Introduction to the interaction between energetic particles and Alfvén eigenmodes in toroidal plasmas. *Rev. Mod. Plasma Phys.* **3**, 1 (2019). URL https://doi.org/10.1007/s41614-018-0022-9

- [13] Heidbrink, W. W. & White, R. B. Mechanisms of energetic-particle transport in magnetically confined plasmas. *Phys. Plasmas* 27, 030901 (2020). URL https://doi.org/10.1063/1.5136237
- [14] Zarzoso, D. et al. Impact of Energetic-Particle-Driven Geodesic Acoustic Modes on Turbulence. Phys. Rev. Lett. 110, 125002 (2013). URL https://doi.org/10.1103/PhysRevLett.110.125002
- [15] Cheng, C. Z. & Chance, M. S. Low-n shear Alfvén spectra in axisymmetric toroidal plasmas. *Phys. Fluids* 29, 3695–3701 (1986). URL https://doi.org/10.1063/1.865801
- [16] Fu, G. Y. & Van Dam, J. W. Excitation of the toroidicity-induced shear Alfvén eigenmode by fusion alpha particles in an ignited tokamak. Phys. Fluids B: Plasma Physics 1, 1949–1952 (1989). URL https://doi.org/10.1063/1.859057
- [17] Pinches, S. D. et al. Energetic ions in ITER plasmas. Phys. Plasmas 22, 021807 (2015). URL https://doi.org/10.1063/1.4908551
- [18] Diamond, P. H., Itoh, S. I., Itoh, K. & Hahm, T. S. Zonal flows in plasmas a review. *Plasma Phys. Control. Fusion* 47, R35 (2005). URL https://doi.org/10.1088/0741-3335/47/5/R01
- [19] Heimpel, M., Aurnou, J. & Wicht, J. Simulation of equatorial and high-latitude jets on Jupiter in a deep convection model. *Nature* 438, 193–196 (2005). URL https://doi.org/10.1038/nature04208
- [20] Todo, Y., Berk, H. L. & Breizman, B. N. Nonlinear magnetohydrodynamic effects on Alfvén eigenmode evolution and zonal flow generation. Nucl. Fusion 50, 084016 (2010). URL https://doi.org/10.1088/ 0029-5515/50/8/084016
- [21] Qiu, Z., Chen, L. & Zonca, F. Effects of energetic particles on zonal flow generation by toroidal Alfvén eigenmode. *Phys. Plasmas* 23, 090702 (2016). URL https://doi.org/10.1063/1.4962997
- [22] Chen, L. & Zonca, F. Physics of Alfvén waves and energetic particles in burning plasmas. Rev. Mod. Phys. 88, 015008 (2016). URL https://doi.org/10.1103/RevModPhys.88.015008
- [23] Breizman, B. N. & Sharapov, S. E. Major minority: energetic particles in fusion plasmas. *Plasma Phys. Control. Fusion* 53, 054001 (2011). URL https://doi.org/10.1088/0741-3335/53/5/054001
- [24] Heidbrink, W. W. Basic physics of Alfvén instabilities driven by energetic particles in toroidally confined plasmas. *Phys. Plasmas* **15**, 055501 (2008). URL https://doi.org/10.1063/1.2838239
- [25] Kazakov, Y. O. et al. Efficient generation of energetic ions in multi-ion plasmas by radio-frequency heating. Nat. Phys. 13, 973-978 (2017). URL https://doi.org/10.1038/nphys4167
- [26] Ongena, J. et al. Synergetic heating of D-NBI ions in the vicinity of the mode conversion layer in H-D plasmas in JET with the ITER like wall. In *EPJ Web Conf.*, vol. 157, 02006 (EDP Sciences, 2017). URL https://doi.org/10.1051/epjconf/201715702006
- [27] Nocente, M. et al. Generation and observation of fast deuterium ions and fusion-born alpha particles in JET D-³He plasmas with the 3-ion radio-frequency heating scenario. Nucl. Fusion **60**, 124006 (2020). URL https://doi.org/10.1088/1741-4326/abb95d
- [28] Kazakov, Y. O. et al. Physics and applications of three-ion ICRF scenarios for fusion research. Phys. Plasmas 28, 020501 (2021). URL https://doi.org/10.1063/5.0021818
- [29] Hawryluk, R. J. An empirical approach to tokamak transport. In Physics of Plasmas Close to Thermonuclear Conditions, 19-46 (Elsevier, 1981). URL https://doi.org/10.1016/B978-1-4832-8385-2.50009-1
- [30] Ongena, J., Voitsekhovitch, I., Evrard, M. & McCune, D. Numerical Transport Codes. Fusion Science and Technology 61, 180–189 (2012). URL https://doi.org/10.13182/FST12-A13505
- [31] Artaud, J. F. et al. The CRONOS suite of codes for integrated tokamak modelling. Nucl. Fusion 50, 043001 (2010). URL https://doi.org/10.1088/0029-5515/50/4/043001
- [32] Garcia, J., Görler, T. & Jenko, F. Isotope and fast ions turbulence suppression effects: Consequences for high-β ITER plasmas. Phys. Plasmas 25, 055902 (2018). URL https://doi.org/10.1063/1.5016331

- [33] Campbell, D. J. et al. Stabilization of sawteeth with additional heating in the JET tokamak. Phys. Rev. Lett. 60, 2148-2151 (1988). URL https://doi.org/10.1103/PhysRevLett.60.2148
- [34] Graves, J. P. et al. Experimental verification of sawtooth control by energetic particles in ion cyclotron resonance heated JET tokamak plasmas. Nucl. Fusion 50, 052002 (2010). URL https://doi.org/10.1088/0029-5515/50/5/052002
- [35] Gates, D. A., Gorelenkov, N. N. & White, R. B. Ion heating by fast-particle-induced Alfvén turbulence. *Phys. Rev. Lett.* 87, 205003 (2001). URL https://doi.org/10.1103/PhysRevLett.87.205003
- [36] Jenko, F., Dorland, W., Kotschenreuther, M. & Rogers, B. N. Electron temperature gradient driven turbulence. Phys. Plasmas 7, 1904–1910 (2000). URL https://doi.org/10.1063/1.874014
- [37] Citrin, J. et al. Electromagnetic stabilization of tokamak microturbulence in a high-β regime. Plasma Phys. Control. Fusion 57, 014032 (2014). URL https://doi.org/10.1088/0741-3335/57/1/014032
- [38] Görler, T. et al. On the Validation of Gyrokinetic L-mode Simulations. Fusion Science and Technology 69, 537–545 (2016). URL https://doi.org/10.13182/FST15-182
- [39] Mazzi, S. et al. Impact of fast ions on a trapped-electron-mode dominated plasma in a JT-60U hybrid scenario. Nucl. Fusion 60, 046026 (2020). URL https://doi.org/10.1088/1741-4326/ab74a1
- [40] Gorelenkov, N. N. et al. Anomalous electron transport due to multiple high frequency beam ion driven Alfvén eigenmodes. Nucl. Fusion 50, 084012 (2010). URL https://doi.org/10.1088/0029-5515/50/8/084012
- [41] Crocker, N. A. et al. Three-wave interactions between fast-ion modes in the national spherical torus experiment. Phys. Rev. Lett. 97, 045002 (2006). URL https://doi.org/10.1103/PhysRevLett.97.045002
- [42] Biglari, H., Diamond, P. H. & Terry, P. W. Influence of sheared poloidal rotation on edge turbulence. *Phys. Fluids B: Plasma Physics* 2, 1–4 (1990). URL https://doi.org/10.1063/1.859529
- [43] Stix, T. H. Heating of toroidal plasmas by neutral injection. *Plasma Phys.* **14**, 367–384 (1972). URL https://doi.org/10.1088/0032-1028/14/4/002

Methods

GENE simulation model and input parameters

In its flux-tube version, the GENE code solves the nonlinear gyrokinetic Vlasov equations [1] coupled to Maxwell's equations on a field-aligned set of spatial coordinates (for a schematic representation, see the top left inset of Figure 1). This system of coordinates allows the exploitation of the strong anisotropy of the turbulent fluctuations in parallel and perpendicular directions to the background magnetic field. Whereas the parallel spatial direction z employs a finite-difference solution technique, the perpendicular direction is treated with spectral methods, and hence the radial x and binormal y coordinates in the Fourier domain are generally referred as k_x and k_y respectively. The two velocity dimensions employed in GENE are the parallel velocity $v_{||}$ and the magnetic moment μ . A detailed description and derivation of the model equations employed in the flux-tube version can be found in Refs. [2, 3].

In the present work, both perpendicular and parallel magnetic field fluctuations are computed, and the collisions are retained. In Gene, Maxwellian distribution functions are employed for all the particle populations, including fast D ions. For the fast ion distribution, effective density and temperature were calculated from the TRANSP distribution. The number of grid points used in the nonlinear simulations is $(n_{k_x} = 256, n_{k_y} = 48, n_z = 32, n_{v_{||}} = 48, n_{\mu} = 64)$ for 4 different particle populations, i.e. electrons, thermal D and ³He ions, and fast D ions. The minimum wavenumber in the binormal direction considered is $k_{y,min}\rho_s = 0.025$. The employed numerical discretization was chosen after extensive convergence tests, even in the nonlinear phase. It must be noted that in the simulations without fast particles, the velocity space has been relaxed to a less demanding numerical grid. Namely, the number of points in the μ -direction has been set to $n_{\mu} = 16$. Indeed, in order to accurately resolve the high-frequency resonances in fast ion velocity space, the non-equidistant Gauss-Legendre discretization in this direction had to be increased up to $n_{\mu} = 64$. Also, for a more comprehensive description of the numerical implementation techniques and adopted schemes employed in Gene, one can consult dedicated Ph.D. theses, e.g. [3], which are available on the Gene website. The input parameters that have been employed in the numerical analyses are reported in Table 1.

The energy flux observable is used to evaluate the radial energy transport computed by the Gene code and compare it with the experimental power balances. The definition of the flux-surface averaged energy flux in the radial direction is:

$$\langle Q_s \rangle = \left\langle \int d^3 v \frac{1}{2} m_s v^2 f_s(\mathbf{x}, \mathbf{v}) \mathbf{v}_{E \times B}(\mathbf{x}) \right\rangle$$

where $\mathbf{x}=(x,y,z)$ and $\mathbf{v}=(v_{\parallel},\mu),\ \langle\cdot\rangle$ denotes the flux-surface average, $f_s(\mathbf{x},\mathbf{v})$ is the distribution function, $\mathbf{v}_{E\times B}=\frac{c}{B_0^2}\mathbf{B}_0\times\nabla\bar{\xi}$ is the generalized $E\times B$ drift velocity, with $\bar{\xi}=\bar{\phi}-\frac{v_{\parallel}}{c}\bar{A}_{\parallel}+\frac{\mu}{q_s}\bar{B}_{\parallel}$ the gyroaveraged modified potential (in which q_s is the charge and the upper bar indicating a gyroaveraged quantity), and the subscript s refers to the species. From this definition, it is possible to appreciate the contributions to the energy flux of the electrostatic potential $\bar{\phi}$, the vector potential \bar{A}_{\parallel} and the parallel magnetic fluctuation \bar{B}_{\parallel} due to the $\mathbf{v}_{E\times B}$ drift. Therefore, it is possible to separate the electrostatic, which includes only the terms with $\bar{\phi}$, and the electromagnetic contributions, which includes the terms with \bar{A}_{\parallel} and \bar{B}_{\parallel} . In addition, it is also possible to determine the flux-surface averaged thermal diffusivities $\langle \chi_s \rangle$ from the energy flux as:

$$\langle \chi_s \rangle = \frac{\langle Q_s \rangle}{n_{0,s} T_{0,s} \omega_{T,s}}$$

where $\omega_{T,s} = -\frac{a}{T_{0,s}} \frac{dT_s}{dx}$ is the normalized temperature gradient of the considered species s. For a more detailed derivation in Gene units of the energy flux and diffusivity, one can consult, e.g., [4].

Interpretive integrated modelling framework

Both pulses #94701 and #94704 were analysed through interpretive simulations performed with the TRANSP modelling suite [5] coupled with external heating modules NUBEAM (NBI) [6] and TORIC (ICRF) [7], and prepared with the OMFIT integrated modelling platform [8]. The interpretive analysis was based on the use of fitted profiles, including electron density and temperature. The fitting procedures for both quantities were based on high resolution Thomson scattering measurements, while the temperature was additionally constrained by electron cyclotron emission data, up to the availability of the experimental measurements. To extrapolate the ion temperature profiles to the magnetic axis, two different approaches were used for pulse #94701: i) assuming $T_i = T_e$ in the region $\rho_{tor} \leq 0.2$ in combination with the available high-resolution T_e data or ii) applying a global

third-order polynomial fit in the range $\rho_{tor} \lesssim 0.8$ (with the additional constraint $\partial T_i(0)/\partial r = 0$). The latter fitting procedure is routinely employed in TRANSP modelling of JET experiments, with as a constraint the consistency between measured and computed quantities such as the neutron rate and the plasma stored energy. Both approaches for pulse #94701 provide very similar results. Indeed, for pulse #94704, only the third-order polynomial fitting procedure has been employed in the TRANSP simulation, with a good agreement (within $\sim 10\%$) with the measured neutron rate. The equilibrium used was an EFIT reconstruction constrained by magnetics and pressure profiles, i.e. including kinetic profiles as well as the contribution of fast ions.

Description of experimental measurements

Mirnov coils are used as a standard MHD diagnostic on almost all tokamak devices. The coils are installed within the vacuum vessel close to the plasma boundary and provide a measurement of the time derivative of the magnetic field. Magnetic spectrograms (Fourier decompositions of the Mirnov coil signal) can then be used to identify relevant oscillation frequencies associated with MHD activity. In JET a number of coil arrays with high frequency response are available, allowing activity in the Alfvén range to be observed. The radial localization of the modes was obtained using an X-mode reflectometer (see Supplementary information). The ion temperature profiles in this paper were obtained from Charge eXchange Recombination Spectroscopy (CXRS) measurements and electron temperature profiles from combined analysis of the electron cyclotron emission (ECE) and high resolution Thomson scattering (HRTS) diagnostics. The density profiles were taken from HRTS measurements, with the density normalized to match the line averaged density measured by a Far Infrared interferometer. The time resolved neutron yield in JET is measured using three fission chambers, containing ²³⁵U and ²³⁸U, located outside the vacuum vessel. The time-of-flight spectrometer for rate (TOFOR) measures the energy distribution of fusion-born neutrons by based on neutron time-of-flight measurements.

Data availability

The JET experimental data is stored in the PPF (Processed Pulse File) system which is a centralised data storage and retrieval system for data derived from raw measurements within the JET Torus, and from other sources such as simulation programs. These data are fully available for the EUROfusion consortium members and can be accessed by non-members under request to EUROfusion.

Numerical data that support the outcome of this study are available from the corresponding author upon reasonable request.

Code availability

The research codes cited in the paper require a prior detailed knowledge of the implemented physics models and are under continuous development. The corresponding author can be contacted for any further information.

References

- [1] Brizard, A. J. & Hahm, T. S. Foundations of nonlinear gyrokinetic theory. Rev. Mod. Phys. 79, 421–468 (2007). URL https://doi.org/10.1103/RevModPhys.79.421.
- [2] Jenko, F., Dorland, W., Kotschenreuther, M. & Rogers, B. N. Electron temperature gradient driven turbulence. Phys. Plasmas 7, 1904–1910 (2000). URL https://doi.org/10.1063/1.874014.
- [3] Merz, F. Gyrokinetic simulation of multimode plasma turbulence. Ph.D. thesis, Universität Münster (2008). URL http://hdl.handle.net/11858/00-001M-0000-0026-FDD2-1.
- [4] Görler, T. Multiscale effects in plasma microturbulence. Ph.D. thesis, Universität Ulm (2009). URL http://dx.doi.org/10.18725/0PARU-1829.
- [5] Ongena, J., Voitsekhovitch, I., Evrard, M. & McCune, D. Numerical Transport Codes. Fusion Science and Technology 61, 180–189 (2012). URL https://doi.org/10.13182/FST12-A13505.

- [6] Pankin, A., McCune, D., Andre, R., Bateman, G. & Kritz, A. The tokamak Monte Carlo fast ion module NUBEAM in the National Transport Code Collaboration library. Comp. Phys. Comm. 159, 157–184 (2004). URL https://doi.org/10.1016/j.cpc.2003.11.002.
- [7] Brambilla, M. Numerical simulation of ion cyclotron waves in tokamak plasmas. *Plasma Phys. Control. Fusion* 41, 1–34 (1999). URL https://doi.org/10.1088/0741-3335/41/1/002.
- [8] Grierson, B. A. et al. Orchestrating TRANSP simulations for interpretative and predictive tokamak modeling with OMFIT. Fusion Science and Technology 74, 101–115 (2018). URL https://doi.org/10.1080/15361055. 2017.1398585.